Translational Oncology
www.transonc.com

Volume 11 Number 5 October 2018 pp. 1065–1073 1065

Molecular Imaging of Pancreatic Duct Adenocarcinoma Using a Type 2 Cannabinoid Receptor-Targeted Near-Infrared Fluorescent Probe

Xiaoxia Guo[*], Xiaoxi Ling[†], Fang Du[‡], Qingbing Wang[*], Wei Huang[*], Zhongmin Wang[*], Xiaoyi Ding[*], Mingfeng Bai[§,¶,#,] and Zhiyuan Wu[*]**

[*]Department of Interventional Radiology, Ruijin Hospital, Shanghai Jiao Tong University School of Medicine, Shanghai 200025, China; [†]Department of Medicine, University of Pittsburgh, 3501 Fifth Ave, Pittsburgh, PA 15213, USA; [‡]Department of Rheumatology, Renji Hospital, Shanghai Jiao Tong University School of Medicine, Shanghai 200025, China; [§]Vanderbilt University Institute of Imaging Science (VUIIS), Vanderbilt University Medical Center, Nashville, TN 37232, USA; [¶]Center for Molecular Probes, Vanderbilt University Medical Center, Nashville, TN 37232, USA; [#]Department of Radiology and Radiological Sciences, Vanderbilt University Medical Center, Nashville, TN 37232, USA; [**]Vanderbilt-Ingram Cancer Center (VICC), Vanderbilt University Medical Center, Nashville, TN 37232, USA

Abstract

Imaging probes targeting type 2 cannabinoid receptor (CB_2R) overexpressed in pancreatic duct adenocarcinoma (PDAC) tissue have the potential to improve early detection and surgical outcome of PDAC. The aim of our study was to evaluate the molecular imaging potential of a CB_2R-targeted near-infrared (NIR) fluorescent probe (NIR760-XLP6) for PDAC. CB_2R overexpression was observed in both PDAC patient tissues and various pancreatic cancer cell lines. *In vitro* fluorescence imaging indicated specific binding of NIR760-XLP6 to CB_2R in human PDAC PANC-1 cells. In a xenograft mouse tumor model, NIR760-XLP6 showed remarkable 50- (*ex vivo*) and 3.2-fold (*in vivo*) tumor to normal contrast enhancement with minimal liver and kidney uptake. In a PDAC lymph node metastasis model, significant signal contrast was observed in bilateral axillary lymph nodes with PDAC metastasis after injection of the probe. In conclusion, NIR760-XLP6 exhibits promising characteristics for imaging PDAC, and CB_2R appears to be an attractive target for PDAC imaging.

Translational Oncology (2018) 11, 1065–1073

Introduction

Pancreatic duct adenocarcinoma (PDAC) is the fourth leading cause of cancer-related death in the United States, with an extremely poor 5-year survival rate of less than 10% and a median survival of 5-8 months after diagnosis [1]. Due to the absence of early symptoms and a lack of accurate diagnostic tools for early-stage detection, only 20% of cases are candidates for surgical resection at the time of diagnosis [2]. Preoperative assessment of PDAC margin status is challenging using current technologies, so even if surgical resection can be performed, most patients have residual disease from margin and therefore recur quickly [3–5]. For patients with advanced disease, treatment options are limited to chemotherapy and radiotherapy, but the effectiveness is unsatisfactory. This is because PDAC is a heterogeneous disease, reflected in diverse clinical response patterns to therapy. Additionally, the tumor hypovasular nature and dense desmoplastic stroma barrier prevent drug delivery [6–8]. Molecular

Address all correspondence to: Xiaoyi Ding or Zhiyuan Wu, Department of Interventional Radiology, Ruijin Hospital, Shanghai Jiao Tong University School of Medicine, Shanghai 200025, China or Mingfeng Bai, Vanderbilt University Institute of Imaging Science (VUIIS), Vanderbilt University Medical Center, Nashville, TN, 37232, USA.
E-mail: wuzhiyuan@shsmu.edu.cn
Received 30 April 2018; Revised 21 June 2018; Accepted 21 June 2018

1936-5233/18
https://doi.org/10.1016/j.tranon.2018.06.009

agents that can specifically target PDAC to allow for early diagnosis and improved therapeutic outcome are therefore in urgent need. To date, though some targets have been explored for PDAC imaging and therapy, such as integrin $\alpha_v\beta_3$, claudin-4, epidermal growth factor receptor, vascular endothelial growth factor receptor, urokinase-type plasminogen activator receptor, carcinoembryonic antigen, and carbohydrate antigen 19-9 (CA19-9), more molecular probes with high PDAC imaging contrast still need to be developed [9–14].

The endogenous cannabinoids system composed of endocannabinoids and two major G protein–coupled receptors (GPCRs), cannabinoid receptor type 1 (CB_1R) and type 2 (CB_2R), plays an important role in various physiological and pathological conditions, making this system an attractive therapeutic target [15–17]. Under basal conditions, CB_1R is highly expressed in the central nervous system and mediates the psychotropic effects of cannabinoids, whereas CB_2R is predominately found in the immune system with high expression only in the spleen and lymph nodes [18–20]. However, many types of cancer, including PDAC, overexpress CB_2R, and the expression levels of CB_2R appear to be associated with tumor aggressiveness [21–25]. Moreover, CB_2R agonists potently inhibited viability, proliferation, adhesion, and migration of various types of cancer cells. Therefore, CB_2R appears to be a promising target for PDAC imaging and therapy.

To date, only a limited number of CB_2R-targeted imaging agents have been reported, which are mainly applied in position emission tomography (PET) imaging [26–28]. Although PET is a great imaging technique for clinical imaging with high sensitivity and deep tissue penetration, it has many limitations, such as relatively low spatial resolution, narrow time window, high instrument cost, and injection of radioactive agents. In contrast, fluorescent imaging is a low-cost imaging method with superior resolution and sensitivity, and is becoming more popularly used in the clinic for diagnostic and surgical navigation purposes. When accompanied with dyes in the near-infrared (NIR) spectrum (650-900 nm) where the interference of high tissue absorption and autofluorescence is minimal, fluorescence imaging can also be used to image deep without any ionizing and radioactive damage [29]. Over the past years, we have developed several CB_2R-targeted fluorescence probes [30–32]. More recently, we reported a new NIR fluorescent probe with high CB_2R-binding affinity and preferential binding selectivity to CB_2R over CB_1R [33]. Here we report the first *in vivo* fluorescence imaging study of PDAC using an NIR CB_2R-targeted exogenous probe.

Materials and Methods

Synthesis of NIR760-XLP6

NIR760-XLP6 was synthesized using our previously reported method [33].

Human Normal and PDAC Tissues

The paired PDAC and normal pancreatic tissues obtained adjacent to the tumors were collected from PDAC patients during surgery at Ruijin Hospital, Shanghai, China. The tissues were frozen immediately in liquid nitrogen and stored in a −80°C freezer until further study. The use of human tissues for the analysis was approved by the local ethical committee (Ruijin Hospital, Shanghai, China), and written informed consent was obtained from the patients.

Reagents

The CB_2R selective ligand 4-quinolone-3-carboxamide (4Q3C) was purchased from Cayman (Ann Arbor, MI). IMDM, DMEM, fetal bovine serum, and penicillin-streptomycin were all purchased from Gibco (Waltham, Ma).

Human PDAC Cell Lines

The human PDAC cell lines CAPAN-1, MIA PaCa-2, BxPC3, PANC-1, and CFPAC-1 were all purchased from ATCC (Manassas, VA). CFPAC-1 cells were cultured in IMDM supplemented with 10% fetal bovine serum and 1% penicillin-streptomycin. The other four cell lines were cultured in DMEM containing 10% fetal bovine serum and 1% penicillin-streptomycin. All cells were grown in an incubator with a constant temperature of 37°C and a humidified atmosphere of 5% CO_2.

Animal Tumor Models

All animal experiments were conducted in accordance with the Guidelines for the Care and Use of Laboratory Animals of Shanghai Jiao Tong University School of Medicine. The xenograft tumor mouse model was developed by injecting 5×10^6 PANC-1 cells into the right flank of 5- to 6-week-old male BALB/c nude mice. The PDAC lymph node metastasis model was induced by the subcutaneous injection of 1×10^6 PANC-1 cells into the hind footpad in nude mice.

Real-Time PCR Analysis

We performed real-time PCR to evaluate CB_2R expression in human PDAC and normal pancreatic tissues, and 5 PDAC cell lines (CAPAN-1, MIA PaCa-2, BxPC3, PANC-1, CFPAC-1). Total RNA was extracted using Trizol reagent (Invitrogen, Carlsbad, CA). The total RNA was reverse transcribed into first-strand cDNA using M-MLV reverse transcriptase (Invitrogen, Carlsbad, CA). The primer sequences set for PCR were as follows: CB_1R (ATGAAGTCGA TCCTAGATGGCCTT and ATGAAGTCGATCCTAGATG GCCTT), CB_2R (CCATGGAGGAATGCTGGGTG and ATCAG ATAGAGCACAGCCACG), and GAPDH (ATGGGGAAGGTGA AGGTCGGAG and GATGACAAGCTTCCCGTTCTCA). GAPDH was used as a housekeeping gene to normalize the relative expression levels. Real-time PCR amplification was performed with SYBR Green PCR Master Mix (Applied Biosystems, Carlsbad, CA) on an ABI 7900 Sequence Detection System using the following conditions: 95°C for 3 minutes and 45 cycles at 95°C for 15 seconds and 60°C for 15 seconds.

Cell Fluorescent Imaging of NIR760-XLP6

PANC-1 cells were divided into three groups: 1) cells treated with 5 μM of NIR760-XLP6 at 37 °C for 30 minutes; 2) cells treated with 5 μM of NIR760-XLP6 at 37°C for 30 minutes after 30 minutes of pretreatment with 10 μM of 4Q3C as the blocking agent; and 3) cells treated with 5 μM of NIR760 at 37°C for 30 minutes. After the incubation, cells were washed three times with PBS and fixed with 4% paraformaldehyde/PBS for 20 minutes at room temperature. The cell nucleus was stained with 1 μg/ml DAPI for 15 minutes at room temperature. Cells were mounted and then imaged using the Zeiss Axio Observer. Z1 fluorescent microscope equipped with the ApoTome 2 imaging system (Carl Zeiss Microimaging Gmbh, Jena, Germany). NIR760-XLP6 or NIR760 fluorescent images were captured using an NIR camera with an ICG filter (excitation/emission: 750-800/820-875 nm). Nuclear images were obtained with a DAPI filter (excitation/emission: 335-383/420-470 nm). Differential interference contrast (DIC) images were obtained through Trans light DIC.

In Vivo Optical Imaging of NIR760-XLP6 in Xenograft Tumor Model

Experiments with tumor-bearing mice were performed 15 days after the injection of tumor cells. A total of 15 mice were divided into 3 groups, each of which was injected with the following agents (dissolved in 100 μl saline) via tail vein: (1) five mice received 10 nmol of NIR760-XLP6, (2) five mice received 100 nmol of 4Q3C followed by 10 nmol of NIR760-XLP6 after 1 hour, and (3) five mice received 10 nmol of NIR760. Mice were anesthetized with 2.5% isoflurane, and images were captured at preinjection and at 0.5, 1, 3, 6, 9, 24, 48, and 72 hours postinjection with a Xenogen IVIS Spectrum imaging system using the following parameters: excitation filter, 745 nm; emission filter, 800 nm; exposure time, 1 second; binning, small; field of view, 12; f/stop, 2; open filter. The signal intensity was expressed as radiant efficiency ([photons/s/cm^2/sr]/[μW/cm^2]). Images were analyzed using Living Image 4.5 software (PerkinElmer). To determine tumor contrast, regions of interest (ROIs) of tumor site at the right flank of the animal (T) and normal tissue at the left flank (N) were drawn. Dividing fluorescence intensity at T by that at N yielded the contrast between the tumor and normal tissue.

Ex Vivo Optical Imaging, Biodistribution, and Histological Study

After the last imaging time point (72 hours postinjection), all mice were sacrificed by cervical dislocation. Tumors and selected organs (heart, lung, liver, spleen, pancreas, kidneys, brain, muscle from left leg, and blood) were excised and imaged using the Xenogen IVIS Spectrum imaging system. The ROIs along the excised tumors and organs were drawn, and the fluorescence intensities were measured. The biodistribution was analyzed by comparing the average fluorescence intensities in the tumor or organs with those in the muscle of left leg from the same animal. For histological study, all excised tumor and organ specimens were fixed in 4% paraformaldehyde and embedded in paraffin for 5-μm tissue sections. After deparaffinization, all sections were stained with hematoxylin and eosin (H&E).

In Vivo and Ex Vivo Optical Imaging in PDAC Lymph Node Metastasis Model

The *in vivo* imaging of NIR760-XLP6 in the PDAC lymph node metastasis mice was performed 5 weeks after the inoculation. Three mice were injected with 10 nmol of NIR760-XLP6 (dissolved in 100 μl saline) via tail vein. Mice were anesthetized with 2.5% isoflurane; images were captured at 0.5, 1, 3, 6, 9, 24, 48 hours postinjection. To determine the lymph node uptake of NIR760-XLP6, the PDAC lymph node metastasis mice were enthanized 48 hours postinjection, and selected lymph nodes, including left proper axillary lymph node, right proper axillary lymph node, left superficial parotid lymph node, and right superficial parotid lymph node, were excised and imaged under Xenogen IVIS Spectrum imaging system. The imaging procedure and image processing method were as described above. To confirm lymph node metastasis, all excised lymph nodes were sectioned for H&E.

Statistical Analysis

All data were presented as mean ± SD (standard error of the mean) of n independent measurements. Statistical analysis was performed using Student's t test (IBM SPSS Statistics version 23). A value of $P < .05$ was considered statistically significant.

Results

CB_2R Expression in Human PDAC Tissues and PDAC Cell Lines

As initial evaluation of whether CB_2R could serve as a potential PDAC target, we quantified the CB_2R expression of human PDAC tissues and cells. Real-time PCR results indicate that the expression level of CB_2R in PDAC tissues was significantly higher than that in normal pancreatic tissues (Figure 1*A*). All PDAC cell lines express both CB_1R and CB_2R, but the expressed levels vary among these cells. Figure 1*B* shows that PANC-1, CAPAN-1, and BxPC3 PDAC cell lines have higher CB_2R expression level than MIA PaCa-2 and CFPAC-1 cell lines. To minimize the interference of CB_1R, we selected PANC-1 cells for our experiments, which have the highest CB_2R/CB_1R expression ratio.

In Vitro Binding Assay of NIR760-XLP6

To evaluate the specificity and imaging potential of NIR760-XLP6 *in vitro*, PANC-1 cells were treated with 5 μM NIR760-XLP6 or NIR760 with or without 4Q3C as the blocking agent. As shown in Figure 2, we observed strong fluorescent signal from cells treated with NIR760-XLP6, which mainly localized in cytoplasm, whereas cells treated with the free dye (NIR760) control failed to show fluorescent

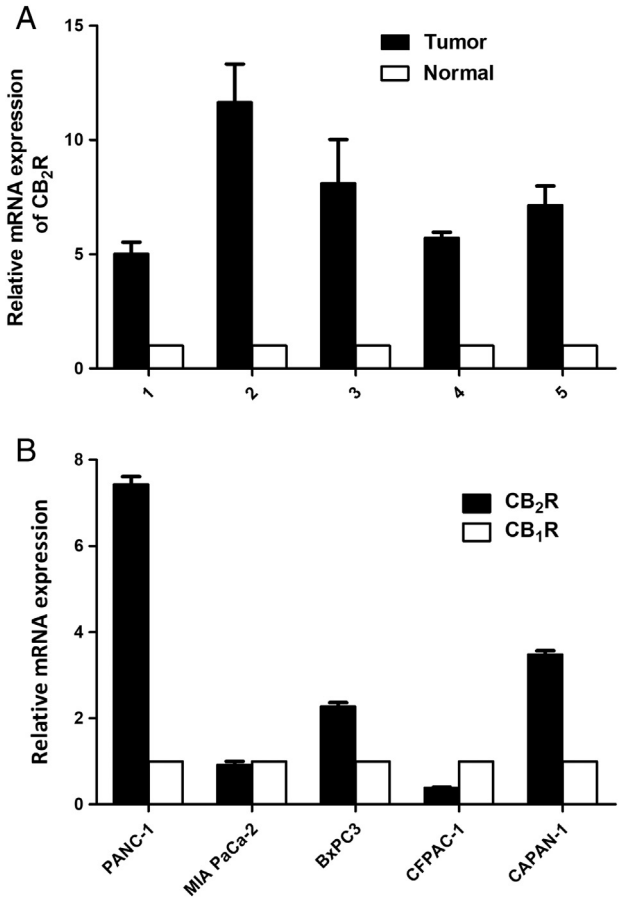

Figure 1. Expression of CB_2R in human PDAC tissues and cell lines. (A) CB_2R expression at the mRNA level was assessed in human PDAC tissues and normal pancreatic tissue samples by real-time PCR. (B) CB_1R and CB_2R expression at the mRNA level was assessed in PDAC cell lines (CAPAN-1, MIA PaCa-2, BxPC3, PANC-1, CFPAC-1) by real-time PCR.

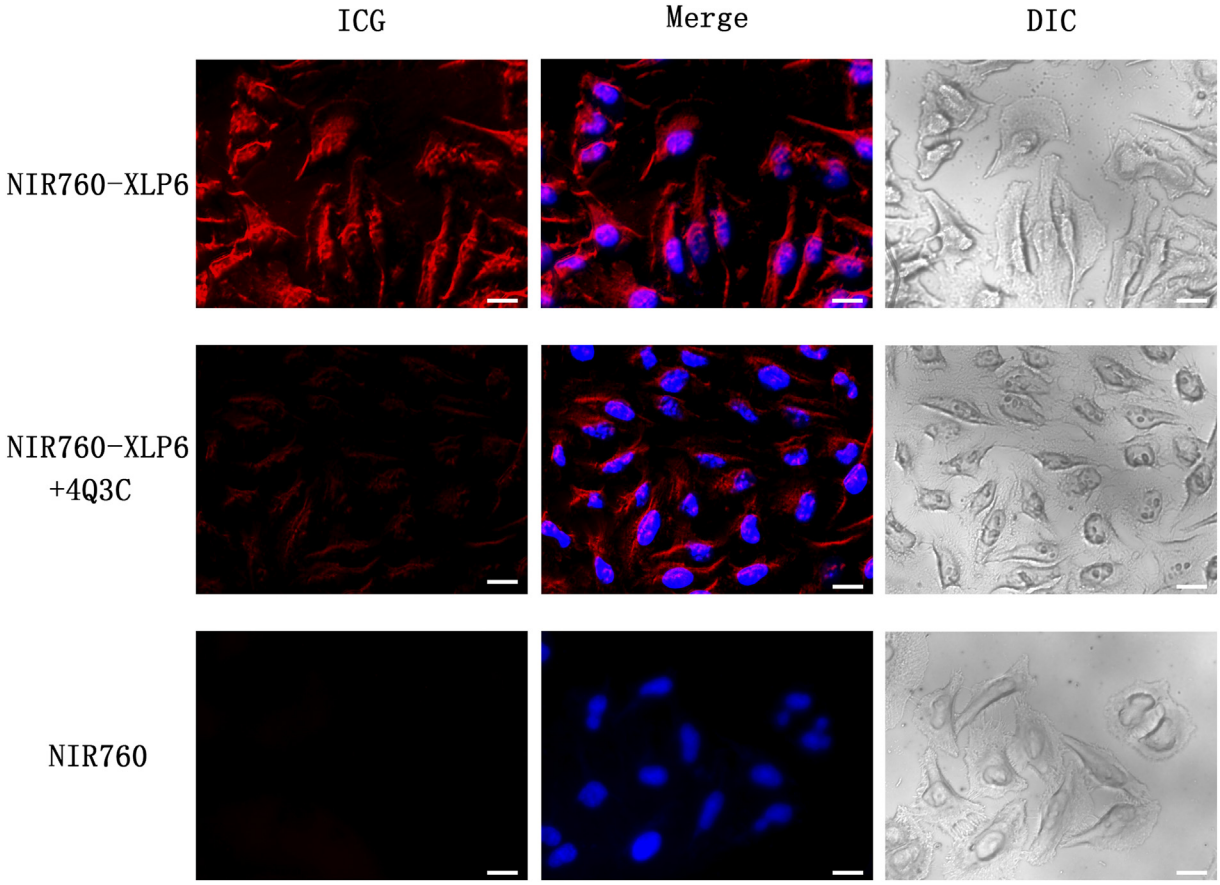

Figure 2. NIR760-XLP6 specifically binds to CB_2R in PANC-1 cells. Cells were divided into three groups as follow: (1) PANC-1 cells treated with NIR760-XLP6; (2) PANC-1 cells treated with 4Q3C followed by NIR760-XLP6; (3) PANC-1 cells treated with NIR760. Fluorescent imaging was obtained using Zeiss Axio Observer fluorescent microscope equipped with the ApoTome 2 imaging system. From left to right, ICG filter (red), ICG filter (red) + DAPI filter (blue) merged, DIC. Scale bars = 20 μm.

signal. In addition, when cells were pretreated with 4Q3C, NIR760-XLP6 showed a much lower degree of cellular uptake compared to unchallenged cells. These fluorescent imaging results indicate specific binding of NIR760-XLP6 to CB_2R.

In Vivo Optical Imaging Studies of NIR760-XLP6 in Xenograft Tumor Model

To study the potential of NIR760-XLP6 for imaging PDAC in living system, we used a xenograft tumor mouse model. *In vivo* optical imaging was performed approximately 15 days postinoculation of PANC-1 cells subcutaneously. The tumor sizes and overall tumor growth in all mice showed no significant difference. A total of 15 mice were divided into 3 groups and administrated with NIR760-XLP6, NIR760-XLP6+ 4Q3C (blocking agent), and NIR760 (nontargeted free dye control), respectively. Figure 3*A* shows the time-dependent fluorescence images of one representative mouse from each group, and all images were displayed on the same scale. Right after the injection, NIR760-XLP6 dispersed rapidly in mice during the first 9 hours and then underwent slow clearance after 24 hours. The tumor of the mouse injected with NIR760-XLP6 showed a visible signal contrast, the T/N ratio gradually increased over time, and the fluorescent signal remained intense even at 72 hours after injection. Comparing the NIR760-XLP6 treatment only group, pretreatment of 4Q3C reduced the T/N ratio at nearly all time points, with statistical significance at 48 hours (2.47 ± 0.07 vs 1.87 ± 0.08, $^{*}P < .05$, respectively) and 72 hours (3.22 ± 0.24 vs 2.25 ± 0.18, $^{*}P < .05$, respectively) postinjection. In contrast, NIR760 exhibited rapid biodistribution within 1 hour postinjection followed by quick tissue clearance without obvious tumor contrast. The T/N ratio of NIR760 was significantly lower than that of NIR760-XLP6 at 48 hours (1.09 ± 0.05 vs 2.47 ± 0.11, $^{***}P < .001$, respectively) and 72 hours (1.09 ± 0.06 vs 3.22 ± 0.41, $^{***}P < .001$, respectively) (Figure 3*B*).

Ex Vivo Imaging, Biodistribution, and Histological Study

After the last imaging time point, *ex vivo* imaging was carried out to study the biodistribution and further evaluate the binding specificity of NIR760-XLP6. Tumor, heart, lung, liver, spleen, pancreas, kidneys, brain, muscle from left leg, and blood were excised and imaged (Figure 4*A*). Remarkably, mice treated with NIR760-XLP6 showed T/N ratio as high as 50, which is significantly higher than the blocking group (49.61 ± 3.92 vs 30.86 ± 6.51, $^{*}P < .05$, respectively). Additionally, the NIR760 group showed much lower tumor contrast than the NIR760-XLP6 treatment group (1.20 ± 0.01 vs 49.61 ± 3.92, $^{***}P < .001$, respectively). Other than the tumors, liver, lung, and kidneys also exhibited comparable signal contrast in both probe and blocking group (liver = 12.28 ± 1.25 vs 11.07 ± 1.37, lung = 13.52 ± 1.24 vs 12.67 ± 1.81, kidneys = 13.48 ± 1.35 vs 10.49 ± 0.53, respectively). Interestingly, the T/N ratios in these organs were much lower than those in tumors, and as expected, no significant blocking effect was observed (Figure 4*B*). These results, along with those from *in vitro* and *in vivo* imaging studies, provide strong evidence on the binding specificity of NIR760-XLP6.

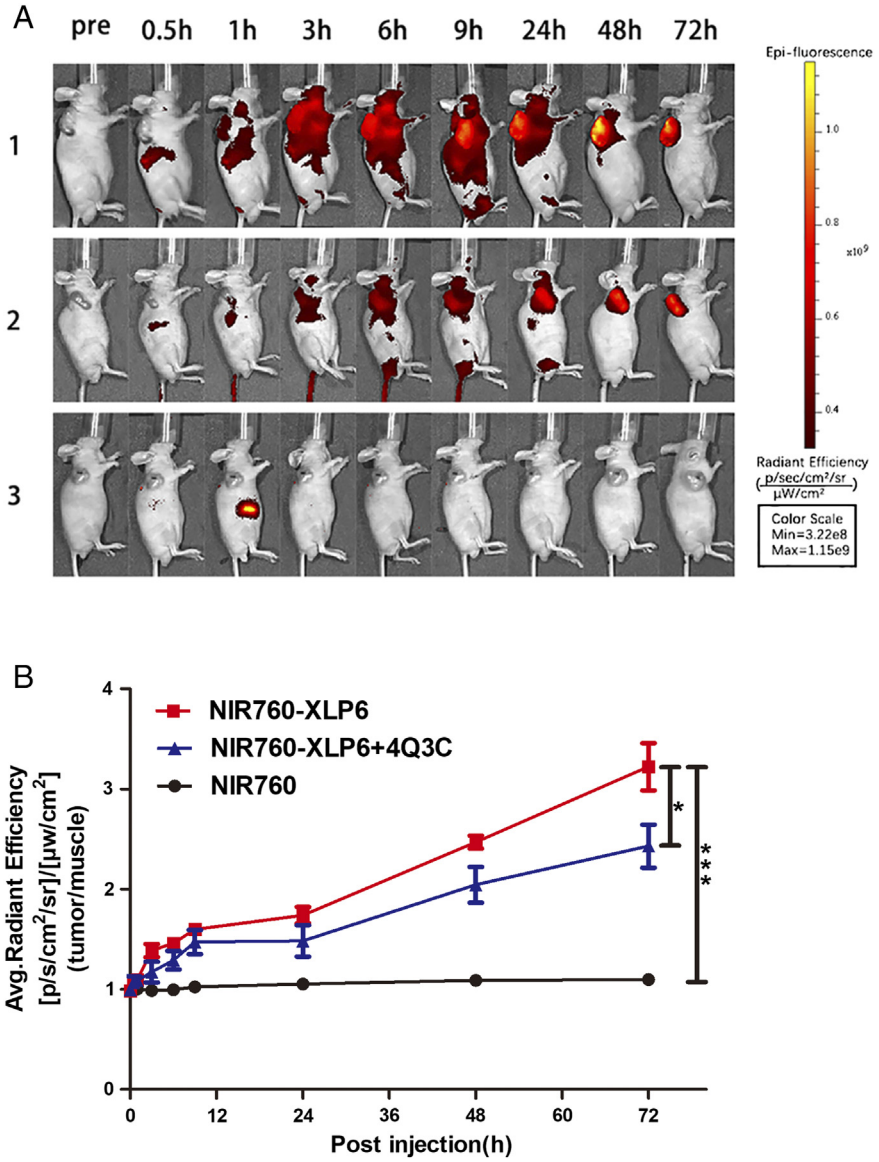

Figure 3. *In vivo* optical imaging of NIR760-XLP6 in xenograft tumor model. All mice were divided into three groups as follows: (1) five PANC-1 tumor-bearing mice injected with NIR760-XLP6; (2) five PANC-1 tumor-bearing mice injected with 4Q3C followed by NIR760-XLP6; (3) five PANC-1 tumor-bearing mice injected with NIR760. (A) Mice were anesthetized and imaged with Xenogen IVIS Spectrum imaging system at preinjection and at 0.5, 1, 3, 6, 9, 24, 48, and 72 hours postinjection. (B) Time activity curves of tumor/normal ratio among three groups. The radiant efficiency of the tumor area at the right flank of the animal (T) and of the area at the left flank normal tissue (N) was calculated by the ROI function in the Living Image software. Dividing T by N yielded the contrast between the tumor tissue and the normal tissue (*$P < .05$, *** $P < .001$).

To determine the gross structure of tumors and examine local toxicity of NIR760-XLP6 in mice, tumors and selected organs (heart, lung, liver, spleen, pancreas, kidneys, brain, and muscle) were sectioned and stained with H&E. Tumor H&E staining images confirmed the presence of human PDAC cells evidenced by the irregularly shaped nucleus with hyperchromatin, polymorphism, and increased mitotic activity (Figure 5*A*). Figure 5*C* shows the representative H&E staining images of organs, and no evidence of inflammation or necrosis from the tissue sections was observed.

In Vivo and Ex Vivo Optical Imaging Study in PDAC Lymph Node Metastasis Model

To further explore the imaging potential of NIR760-XLP6 for PDAC, we performed *in vivo* optical imaging in lymph node metastasis mice. Three mice were treated with 100 nmol of NIR760-XLP6. One representative mouse was shown, and all images were displayed on the same scale (Figure 6*A*). Upon injection, visible signal contrast was observed in bilateral axilla and bladder region; the signal contrast reached maximum rapidly at 3 hours postinjection and then underwent a delayed clearance after 9 hours. To study the biodistribution of NIR760-XLP6 in lymph nodes, all mice were euthanized after the last imaging time point; selected lymph nodes (left proper axillary lymph node, right proper axillary lymph node, left superficial parotid lymph node, and right superficial parotid lymph node) were excised and imaged (Figure 6*B*). Lymph nodes exhibited significant signal contrast, but lower to bladder (3.34±0.53 vs 5.03±0.79 3.58±1.39 vs 5.03±0.79 3.24±0.53 vs 5.03±0.79 2.76±0.31 vs 5.03±0.79, respectively), this maybe because the probe is excreted

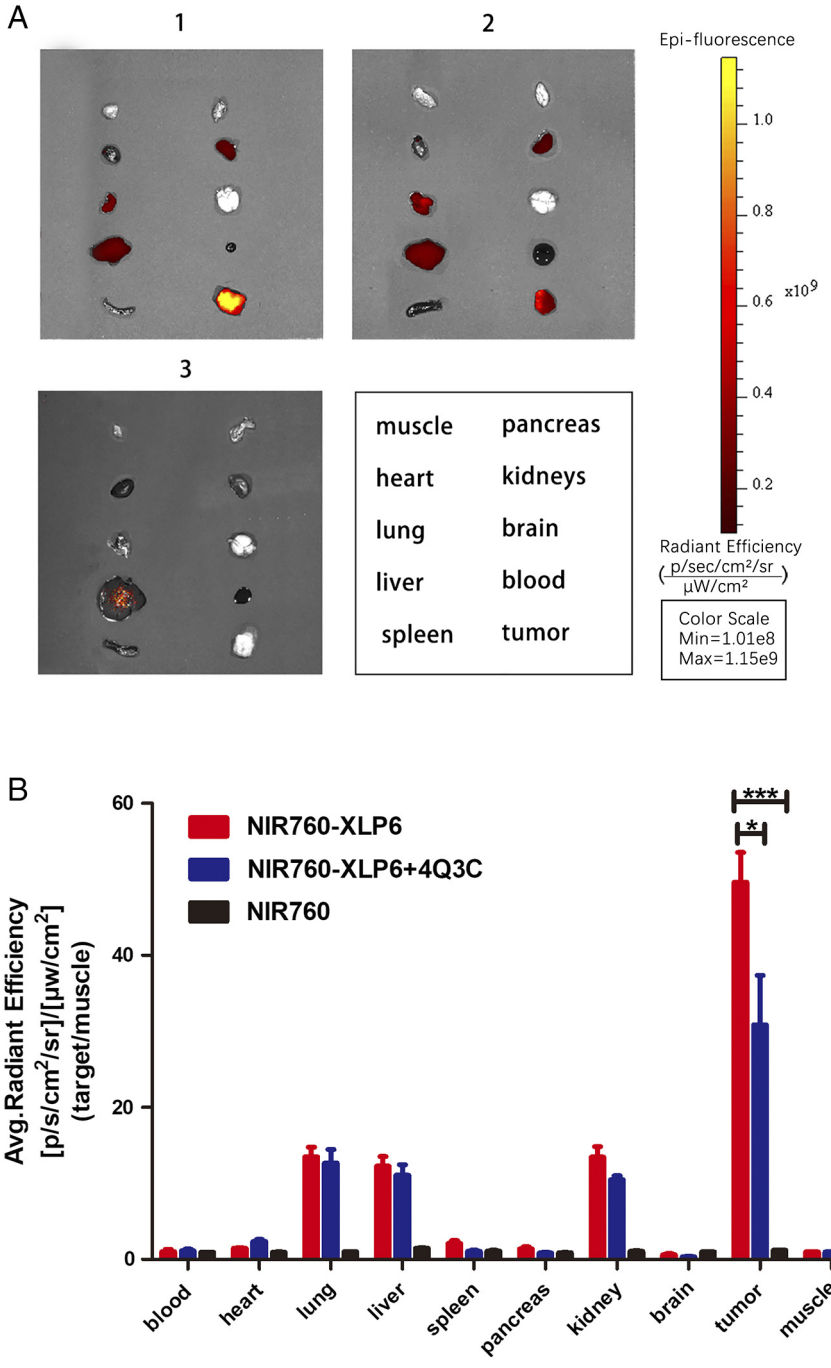

Figure 4. *Ex vivo* tumor optical imaging and biodistribution study of NIR760-XLP6. All mice were divided into three groups as follows: (1) five PANC-1 tumor-bearing mice injected with NIR760-XLP6; (2) five PANC-1 tumor-bearing mice injected with 4Q3C followed by NIR760-XLP6; (3) five PANC-1 tumor-bearing mice injected with NIR760. (A) *Ex vivo* imaging of excised tumor and organs at 72 hours postinjection from PANC-1 tumor-bearing mice. (B) Graphical quantification of target/normal signal ratios among the three groups (*$P < .05$, *** $P < .001$).

through the bladder. Subsequently, we performed H&E to confirm lymph nodes and metastatic lymph nodes. Figure 5*B* shows a representative H&E staining image of metastatic lymph node.

Discussion

To our best knowledge, this is the first report on CB_2R-targeted NIR fluorescence imaging of PDAC. Much effort has been spent on exploring highly specific molecular target of PDAC to improve the diagnosis and treatment of this dismal disease in the past decade. However, long blood circulation times and suboptimal tumor accumulation constrained their potential clinical application [34,35]; effective therapy has only been shown in few examples in experimental pancreatic tumor models, including nanomedicines targeting the epidermal growth factor, integrin $\alpha_v\beta_3$ receptor, and transferrin receptor [36–39]. In this study, we demonstrate that an NIR probe (NIR760-XLP6) specifically binds to CB_2R in PANC-1 cells and tumors and led to high imaging contrast (3.2-fold *in vivo* and 50-fold ex vivo) with minimal uptake in organs. These encouraging results suggest that NIR760-XLP6 may have great potential in imaging PDAC using low-cost fluorescence imaging systems.

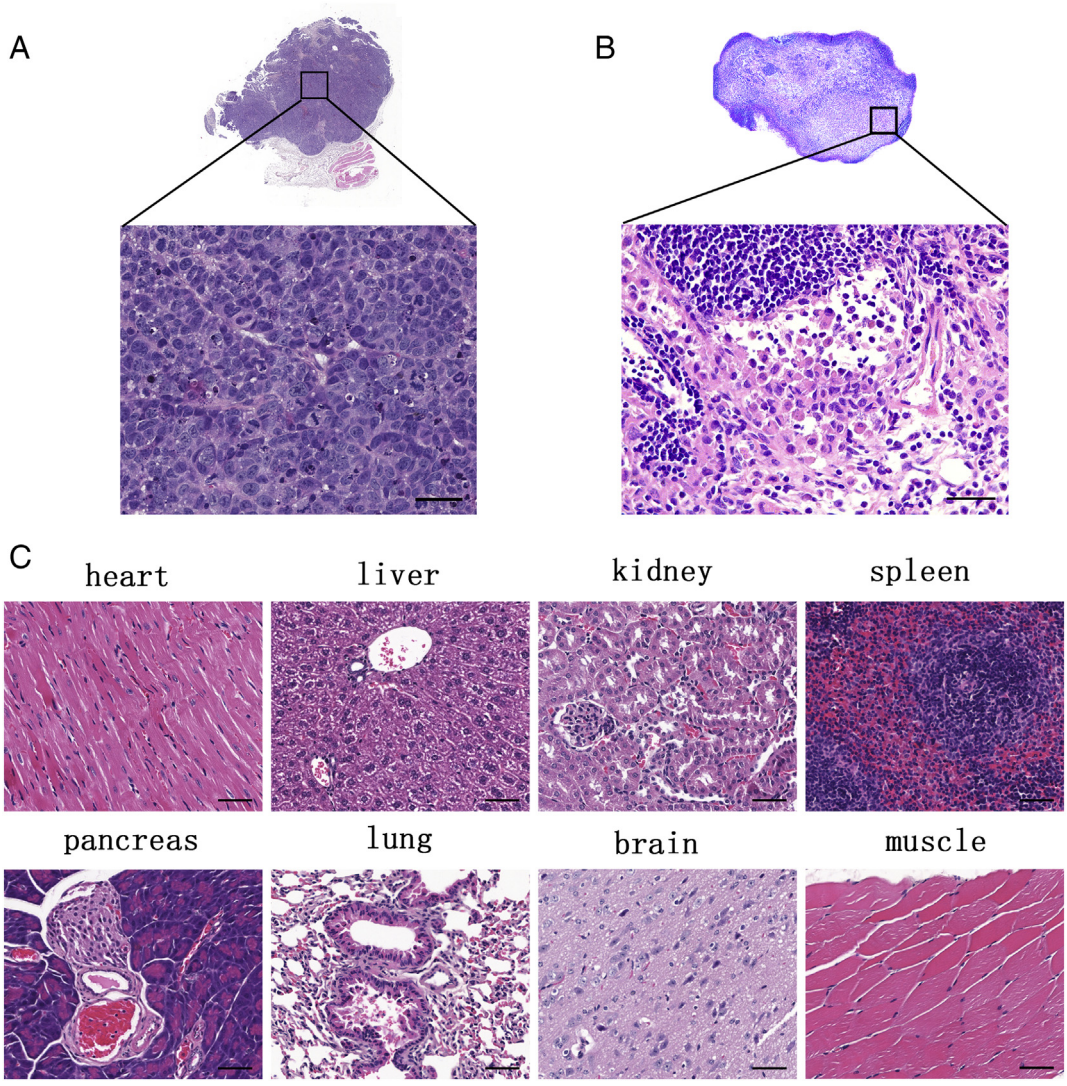

Figure 5. Representative histological images of excised tumor, the major organs, and lymph node from mice postinjected with NIR760-XLP6. (A) Tumor H&E staining image. (B) Metastatic lymph node H&E staining image. (C) The major organs' H&E staining images. Scale bars = 50 μm.

High overexpression level is of critical importance to a target candidate for diagnostic and therapeutic purposes. We therefore performed real-time PCR to quantify the expression of CB_2R in patient PDAC samples as compared to normal pancreas tissues. We found that CB_2R was highly overexpressed in randomly selected patient samples. This is consistent with previous studies, which have demonstrated strong upregulation of CB_2R in various cancers, including pancreatic cancer, whereas it is undetectable or expressed at rather low levels in the corresponding normal tissues [21, 40]. In additional to patient samples, we also examined CB_2R expression in five PDAC cell lines and found CB_2R expression in all tested cell lines, with high level in PANC-1, CAPAN-1, and BxPC3 PDAC cells and relatively low level in MIA PaCa-2 and CFPAC-1 cell lines. The overexpression of CB_2R in PDAC patient samples and cell lines suggests that CB_2R is a promising target for PDAC.

Cellular fluorescence imaging showed that NIR760-XLP6 primarily localized in the cytoplasm of PANC-1 cells, which is seemingly unexpected as CB_2R belongs to transmembrane GPCR family. However, this observation is consistent with recent studies reported by us and others that CB2R is primarily located at intracellular sites in certain cell lines [41–43]. This may be contributed to ligand-induced internalization, which is part of membrane trafficking of GPCR in regulating complex signaling pathways [44]. Recent studies have shown that CB_2R underwent internalization after sustained exposure to agonists [42, 43]. When blocked with 4Q3C, NIR760-XLP6 showed a much lower degree of cell uptake. Furthermore, cells treated with free dye did not show significantly fluorescence signal. These results are similar to our previously reported cellular imaging studies using DBT-CB2 cells, indicating that NIR760-XLP6 specifically binds to CB_2R [33].

Building upon the findings from cellular imaging studies, we further evaluated the *in vivo* imaging potential of NIR760-XLP6 in PANC-1 tumor-bearing mice. Free dye control mice showed rapid biodistribution and quick bioclearance throughout the whole bodies without tumor contrast. Conversely, significant fluorescence signal was observed in the mice injected with NIR760-XLP6, and the T/N ratio increased gradually over time. In addition, blocking agent 4Q3C partially decreased the uptake of NIR760-XLP6 in tumors. Although we collected similar results in our previous study using the same probe and the DBT-CB2 tumor mouse model, the imaging contrast shown in this study is far more remarkable. Specifically, T/N ratios of 2.0 (*in vivo*) and 7.9 (ex vivo)

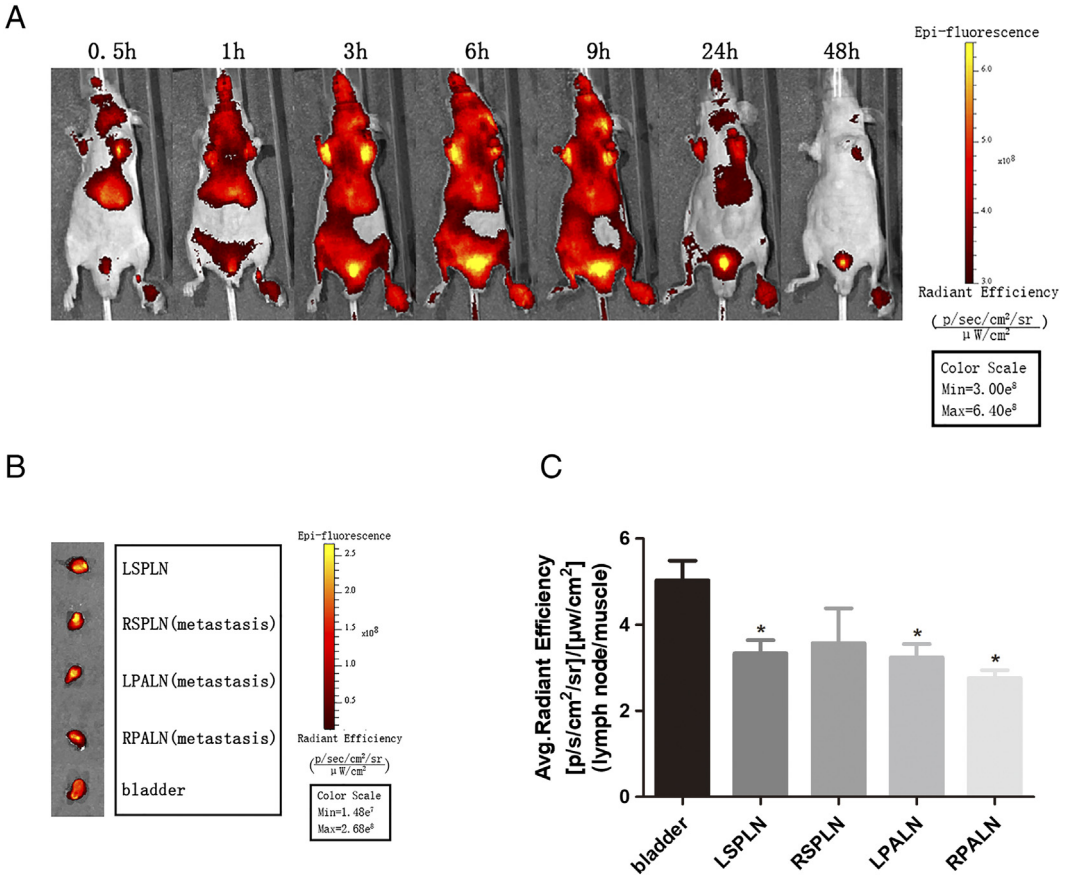

Figure 6. *In vivo* and *ex vivo* optical imaging of NIR760-XLP6 in PDAC lymph node metastasis model. (A) Three PDAC lymph node metastasis mice were injected with NIR760-XLP6 and imaged with Xenogen IVIS Spectrum imaging system at 0.5, 1, 3, 6, 9, 24, and 48 hours postinjection. (B) *Ex vivo* imaging of lymph nodes at 48 hours postinjection from PDAC lymph node metastasis mice. (C) Graphical quantification of target/normal signal ratios among lymph nodes (*$P < .05$).

were recorded in our previous study, whereas T/N ratios as high as 3.2 (*in vivo*) and 49.6 (ex vivo) were observed here. This is likely due to the high expression level of CB_2R in PANC-1 tumors as compared to DBT-CB2 cells that are delayed brain tumor cells transfected to express CB_2R at a medium (endogenous) level. We also found that mice injected with NIR760-XLP6 showed no local toxicity in major organs based on the H&E staining. The safety profile and high imaging contrast provide strong support on the potential of NIR760-XLP6 as a new PDAC imaging probe.

To further explore the imaging potential of NIR760-XLP6 for PDAC, we performed *in vivo* imaging of NIR760-XLP6 in PDAC lymph node metastasis mice. After injection of the probe, significant signal contrast was observed in bilateral axilla at all time points, especially 3, 6, and 9 hours postinjection, which were confirmed to be proper axillary lymph node with PDAC metastasis by H&E. Meanwhile, the T/N ratios of approximately 3.0 (*ex vivo*) were obtained 48 hours postinjection in both metastatic lymph nodes and normal lymph nodes. The distinct fluorescent signal of normal lymph nodes may be due to the high expression of CB_2R in normal lymph nodes. Indeed, in basal conditions, CB_2R is highly expressed in spleen and lymph nodes. There is literature reported that a significant fluorescent signal was observed in spleen 1 hour postinjection using a similar CB_2R-targeted probe [45]. However, the fluorescent intensities of lymph nodes and spleen were all remarkably lower to tumors. These findings further confirmed the potential of NIR760-XLP6 to image PDAC.

Conclusion

In conclusion, we successfully imaged PDAC cells and tumors using our CB_2R-targeted NIR fluorescent probe, NIR760-XLP6. Our results suggest that CB_2R is a promising target for PDAC imaging. We plan to embark on CB_2R-targeted PDAC imaging using more sophisticated tumor models, for example, comparing the imaging effect of NIR760-XLP6 in PDAC lymph node metastasis model to inflammation model, as well as further exploring the potential of cannabinoid therapy for PDAC in our future studies.

Funding

This study was sponsored by Shanghai Pujiang Program (16PJ1406200) and Scientific Research Innovation Projects of Shanghai Municipal Education Commission (15ZZ060).

References

[1] Siegel RL, Miller KD, and Jemal A (2017). Cancer statistics, 2017. *CA Cancer J Clin* **67**, 7–30.

[2] Kamisawa T, Wood LD, Itoi T, and Takaori K (2016). Pancreatic cancer. *Lancet* **388**, 73–85.

[3] Gillen S, Schuster T, Meyer Zum Buschenfelde C, Friess H, and Kleeff J (2010). Preoperative/neoadjuvant therapy in pancreatic cancer: a systematic review and meta-analysis of response and resection percentages. *PLoS Med* **7**, e1000267.

[4] Konstantinidis IT, Warshaw AL, Allen JN, Blaszkowsky LS, Castillo CF, Deshpande V, Hong TS, Kwak EL, Lauwers GY, and Ryan DP, et al (2013). Pancreatic ductal

adenocarcinoma: is there a survival difference for R1 resections versus locally advanced unresectable tumors? What is a "true" R0 resection? *Ann Surg* **257**, 731–736.
[5] Frampton AE, Gall TM, Krell J, Ahmad R, and Jiao LR (2013). Is there a 'margin' for error in pancreatic cancer surgery? *Future Oncol* **9**, 31–34.
[6] Provenzano PP and Hingorani SR (2013). Hyaluronan, fluid pressure, and stromal resistance in pancreas cancer. *Br J Cancer* **108**, 1–8.
[7] Wolfgang CL, Herman JM, Laheru DA, Klein AP, Erdek MA, Fishman EK, and Hruban RH (2013). Recent progress in pancreatic cancer. *CA Cancer J Clin* **63**, 318–348.
[8] Iovanna J and Dusetti N (2017). Speeding towards individualized treatment for pancreatic cancer by taking an alternative road. *Cancer Lett* **410**, 63–67.
[9] Neesse A, Hahnenkamp A, Griesmann H, Buchholz M, Hahn SA, Maghnouj A, Fendrich V, Ring J, Sipos B, and Tuveson DA, et al (2013). Claudin-4-targeted optical imaging detects pancreatic cancer and its precursor lesions. *Gut* **62**, 1034–1043.
[10] Trajkovic-Arsic M, Mohajerani P, Sarantopoulos A, Kalideris E, Steiger K, Esposito I, Ma X, Themelis G, Burton N, and Michalski CW, et al (2014). Multimodal molecular imaging of integrin alphavbeta3 for in vivo detection of pancreatic cancer. *J Nucl Med* **55**, 446–451.
[11] Luo H, England CG, Goel S, Graves SA, Ai F, Liu B, Theuer CP, Wong HC, Nickles RJ, and Cai W (2017). ImmunoPET and near-infrared fluorescence imaging of pancreatic cancer with a dual-labeled bispecific antibody fragment. *Mol Pharm* **14**, 1646–1655.
[12] Li H, Wang P, Gong W, Wang Q, Zhou J, Zhu WH, and Cheng Y (2017). Dendron-grafted polylysine-based dual-modal nanoprobe for ultra-early diagnosis of pancreatic precancerosis via targeting a urokinase-type plasminogen activator receptor. *Adv Healthc Mater* **7**. doi:10.1002/adhm.201700912 1700912 (1 to 9).
[13] Lwin TM, Murakami T, Miyake K, Yazaki PJ, Shivley JE, Hoffman RM, and Bouvet M (2018). Tumor-specific labeling of pancreatic cancer using a humanized anti-CEA antibody conjugated to a near-infrared fluorophore. *Ann Surg Oncol* **25**, 1079–1085.
[14] Hudson SV, Huang JS, Yin W, Albeituni S, Rush J, Khanal A, Yan J, Ceresa BP, Frieboes HB, and McNally LR (2014). Targeted noninvasive imaging of EGFR-expressing orthotopic pancreatic cancer using multispectral optoacoustic tomography. *Cancer Res* **74**, 6271–6279.
[15] Aizpurua-Olaizola O, Elezgarai I, Rico-Barrio I, Zarandona I, Etxebarria N, and Usobiaga A (2017). Targeting the endocannabinoid system: future therapeutic strategies. *Drug Discov Today* **22**, 105–110.
[16] Matsuda LA, Lolait SJ, Brownstein MJ, Young AC, and Bonner TI (1990). Structure of a cannabinoid receptor and functional expression of the cloned cDNA. *Nature* **346**, 561–564.
[17] Munro S, Thomas KL, and Abu-Shaar M (1993). Molecular characterization of a peripheral receptor for cannabinoids. *Nature* **365**, 61–65.
[18] Volkow ND, Baler RD, Compton WM, and Weiss SR (2014). Adverse health effects of marijuana use. *N Engl J Med* **370**, 2219–2227.
[19] Deng L, Guindon J, Cornett BL, Makriyannis A, Mackie K, and Hohmann AG (2015). Chronic cannabinoid receptor 2 activation reverses paclitaxel neuropathy without tolerance or cannabinoid receptor 1-dependent withdrawal. *Biol Psychiatry* **77**, 475–487.
[20] Galiegue S, Mary S, Marchand J, Dussossoy D, Carriere D, Carayon P, Bouaboula M, Shire D, Le Fur G, and Casellas P (1995). Expression of central and peripheral cannabinoid receptors in human immune tissues and leukocyte subpopulations. *Eur J Biochem* **232**, 54–61.
[21] Carracedo A, Gironella M, Lorente M, Garcia S, Guzman M, Velasco G, and Iovanna JL (2006). Cannabinoids induce apoptosis of pancreatic tumor cells via endoplasmic reticulum stress-related genes. *Cancer Res* **66**, 6748–6755.
[22] Dando I, Donadelli M, Costanzo C, Dalla Pozza E, D'Alessandro A, Zolla L, and Palmieri M (2013). Cannabinoids inhibit energetic metabolism and induce AMPK-dependent autophagy in pancreatic cancer cells. *Cell Death Dis* **4**, e664.
[23] Vara D, Salazar M, Olea-Herrero N, Guzman M, Velasco G, and Diaz-Laviada I (2011). Anti-tumoral action of cannabinoids on hepatocellular carcinoma: role of AMPK-dependent activation of autophagy. *Cell Death Differ* **18**, 1099–1111.
[24] Casanova ML, Blazquez C, Martinez-Palacio J, Villanueva C, Fernandez-Acenero MJ, Huffman JW, Jorcano JL, and Guzman M (2003). Inhibition of skin tumor growth and angiogenesis in vivo by activation of cannabinoid receptors. *J Clin Invest* **111**, 43–50.
[25] Morales P, Blasco-Benito S, Andradas C, Gomez-Canas M, Flores JM, Goya P, Fernandez-Ruiz J, Sanchez C, and Jagerovic N (2015). Selective, nontoxic CB(2) cannabinoid o-quinone with in vivo activity against triple-negative breast cancer. *J Med Chem* **58**, 2256–2264.
[26] Evens N and Bormans GM (2010). Non-invasive imaging of the type 2 cannabinoid receptor, focus on positron emission tomography. *Curr Top Med Chem* **10**, 1527–1543.
[27] Caille F, Cacheux F, Peyronneau MA, Jego B, Jaumain E, Pottier G, Ullmer C, Grether U, Winkeler A, and Dolle F, et al (2017). From structure-activity relationships on thiazole derivatives to the in vivo evaluation of a new radiotracer for cannabinoid subtype 2 PET imaging. *Mol Pharm* **14**, 4064–4078.
[28] Evens N, Vandeputte C, Muccioli GG, Lambert DM, Baekelandt V, Verbruggen AM, Debyser Z, Van Laere K, and Bormans GM (2011). Synthesis, in vitro and in vivo evaluation of fluorine-18 labelled FE-GW405833 as a PET tracer for type 2 cannabinoid receptor imaging. *Bioorg Med Chem* **19**, 4499–4505.
[29] Frangioni J (2003). In vivo near-infrared fluorescence imaging. *Curr Opin Chem Biol* **7**, 626–634.
[30] Wu Z, Shao P, Zhang S, Ling X, and Bai M (2014). Molecular imaging of human tumor cells that naturally overexpress type 2 cannabinoid receptors using a quinolone-based near-infrared fluorescent probe. *J Biomed Opt* **19**76016.
[31] Zhang S, Shao P, and Bai M (2013). In vivo type 2 cannabinoid receptor-targeted tumor optical imaging using a near infrared fluorescent probe. *Bioconjug Chem* **24**, 1907–1916.
[32] Wu Z, Shao P, Zhang S, and Bai M (2014). Targeted zwitterionic near infrared fluorescent probe for improved imaging of type 2 cannabinoid receptors. *J Biomed Opt* **19**36006.
[33] Ling X, Zhang S, Shao P, Li W, Yang L, Ding Y, Xu C, Stella N, and Bai M (2015). A novel near-infrared fluorescence imaging probe that preferentially binds to cannabinoid receptors CB2R over CB1R. *Biomaterials* **57**, 169–178.
[34] Aung W, Tsuji AB, Sudo H, Sugyo A, Furukawa T, Ukai Y, Kurosawa Y, and Saga T (2016). Immunotargeting of integrin alpha6beta4 for single-photon emission computed tomography and near-infrared fluorescence imaging in a pancreatic cancer model. *Mol Imaging* **15**. doi:10.1177/1536012115624917.
[35] Huynh AS, Chung WJ, Cho HI, Moberg VE, Celis E, Morse DL, and Vagner J (2012). Novel toll-like receptor 2 ligands for targeted pancreatic cancer imaging and immunotherapy. *J Med Chem* **55**, 9751–9762.
[36] Camp ER, Wang C, Little EC, Watson PM, Pirollo KF, Rait A, Cole DJ, Chang EH, and Watson DK (2013). Transferrin receptor targeting nanomedicine delivering wild-type p53 gene sensitizes pancreatic cancer to gemcitabine therapy. *Cancer Gene Ther* **20**, 222–228.
[37] Salvati A, Pitek AS, Monopoli MP, Prapainop K, Bombelli FB, Hristov DR, Kelly PM, Aberg C, Mahon E, and Dawson KA (2013). Transferrin-functionalized nanoparticles lose their targeting capabilities when a biomolecule corona adsorbs on the surface. *Nat Nanotechnol* **8**, 137–143.
[38] Kudgus RA, Szabolcs A, Khan JA, Walden CA, Reid JM, Robertson JD, Bhattacharya R, and Mukherjee P (2013). Inhibiting the growth of pancreatic adenocarcinoma in vitro and in vivo through targeted treatment with designer gold nanotherapeutics. *PLoS One* **8**e57522.
[39] Ji S, Xu J, Zhang B, Yao W, Xu W, Wu W, Xu Y, Wang H, Ni Q, and Hou H, et al (2012). RGD-conjugated albumin nanoparticles as a novel delivery vehicle in pancreatic cancer therapy. *Cancer Biol Ther* **13**, 206–215.
[40] Michalski CW, Oti FE, Erkan M, Sauliunaite D, Bergmann F, Pacher P, Batkai S, Muller MW, Giese NA, and Friess H, et al (2008). Cannabinoids in pancreatic cancer: correlation with survival and pain. *Int J Cancer* **122**, 742–750.
[41] Zhang S, Jia N, Shao P, Tong Q, Xie XQ, and Bai M (2014). Target-selective phototherapy using a ligand-based photosensitizer for type 2 cannabinoid receptor. *Chem Biol* **21**, 338–344.
[42] Castaneda JT, Harui A, Kiertscher SM, Roth JD, and Roth MD (2013). Differential expression of intracellular and extracellular CB(2) cannabinoid receptor protein by human peripheral blood leukocytes. *J Neuroimmune Pharmacol* **8**, 323–332.
[43] Atwood BK, Wager-Miller J, Haskins C, Straiker A, and Mackie K (2011). Functional selectivity in CB2 cannabinoid receptor signaling and regulation: implications for the therapeutic potential of CB2 ligands. *Mol Pharmacol* **81**, 250–263.
[44] Jean-Alphonse F and Hanyaloglu AC (2011). Regulation of GPCR signal networks via membrane trafficking. *Mol Cell Endocrinol* **331**, 205–214.
[45] Zhang S, Shao P, Ling X, Yang L, Hou W, Thorne SH, Beaino W, Anderson CJ, Ding Y, and Bai M (2015). In vivo inflammation imaging using a CB2R-targeted near infrared fluorescent probe. *Am J Nucl Med Mol Imaging* **5**, 246–258.